

# Design of a Mott Multiferroic from a Non-Magnetic Polar Metal

Danilo Puggioni,<sup>1</sup> Gianluca Giovannetti,<sup>2</sup> Massimo Capone,<sup>2</sup> and James M. Rondinelli<sup>1</sup>

<sup>1</sup>*Department of Materials Science and Engineering, Northwestern University, IL 60208-3108, USA*

<sup>2</sup>*CNR-IOM-Democritos National Simulation Centre and International School for Advanced Studies (SISSA), Trieste, Italy*

We examine the electronic properties of newly discovered “ferroelectric” metal  $\text{LiOsO}_3$  combining density-functional and dynamical mean-field theories. We show that the material is close to a Mott transition and that electronic correlations can be tuned to engineer a Mott multiferroic state in 1/1 superlattice of  $\text{LiOsO}_3$  and  $\text{LiNbO}_3$ . We use electronic structure calculations to predict that the  $(\text{LiOsO}_3)_1/(\text{LiNbO}_3)_1$  superlattice is a type-I multiferroic material with a ferroelectric polarization of  $41.2 \mu\text{C cm}^{-2}$ , Curie temperature of 927 K, and Néel temperature of 671 K. Our results support a route towards high-temperature multiferroics, *i.e.*, driving non-magnetic *polar metals* into correlated insulating magnetic states.

PACS numbers: 75.85.+t, 71.45.Gm, 77.80.B-, 71.20.-b,

**Introduction.**—Multiferroics (MF) are a class of insulating materials where two (or more) primary ferroic order parameters, such as a ferroelectric polarization and long-range magnetic order, coexist. Technologically, they offer the possibility to control magnetic polarizations with an electric field for reduced power consumption [1, 2]. Nonetheless, intrinsic room-temperature MF remain largely elusive. This fact may be understood by examining the microscopic origins for the ferroic order which aids in classifying different phases: In Type-I MF, ferroelectricity and magnetism arise from different chemical species with ordering temperatures largely independent of one another and weak magnetoelectric (ME) coupling [3]. The ferroelectric ordering also typically appears at temperatures higher than the magnetic order, and the spontaneous polarization  $P$  is large since it is driven by a second-order Jahn-Teller distortion, *e.g.*,  $\text{BiFeO}_3$  [3, 4]. In Type-II MF, however, magnetic order induces ferroelectricity, which indicates a strong ME coupling between the two order parameters. Nonetheless,  $P$  is usually much smaller, *e.g.*, by a factor of  $10^2$  as in  $R\text{-Mn}_2\text{O}_5$  ( $R$  being rare earth) [5]. In a few MFs with high-transition temperatures, *i.e.*,  $\text{BiFeO}_3$  [6] and  $\text{Sr}_{1-x}\text{Ba}_x\text{MnO}_3$  [7–9], magnetism is caused by Mott physics arising from strong correlations. The interactions localize the spins at high temperature, paving the way for magnetic ordering at room temperature. Materials where this robust magnetism is coupled with ferroelectric distortions are ideal candidates for a room-temperature MFs.

Herein, we propose a design strategy for novel Mott MF phases. It relies on tuning the degree of correlation of the recently discovered class of materials referred to as ‘ferroelectric metals’ with  $\text{LiOsO}_3$  as the prototypical member [10]. This material is the first undisputed realization of the Anderson-Blount mechanism [11], and challenges the expectation that conduction electrons in metals would screen the electric field induced by polar displacements [10, 12, 13]. Despite robust metallicity, this material shares structural similarities with prototypical *insulating* ferroelectric oxides, such as  $\text{LiNbO}_3$  [14, 15]: A

$R3c$  crystal structure with acentric cation displacements and distorted  $\text{OsO}_6$  octahedra [16, 17] and comparable lattice parameters [10, 14]. While the *polar displacements* in  $\text{LiNbO}_3$  rely on cross-gap hybridization between  $p$  (O) and  $d$  (Nb) states [18], in  $\text{LiOsO}_3$  they are weakly coupled to the states at the Fermi level ( $E_F$ ), which makes possible the coexistence of an acentric structure and metallicity [16, 19]. In  $\text{LiOsO}_3$  the empty  $d$ -manifold of  $\text{LiNbO}_3$  is replaced by a non-magnetic  $5d^3$  ground state with a half-filled  $t_{2g}$  ( $d_{xy}, d_{xz}, d_{yz}$ ) configuration, which is responsible for the metallic response [16]. However, the strength of the electronic interactions is insufficient to drive a Mott transition in the correlated  $t_{2g}$  manifold as revealed by low-temperature resistivity measurements; nonetheless, if it would be possible to enhance the electronic correlations in  $\text{LiOsO}_3$  and achieve a metal-insulator transition, then a previously unidentified multiferroic material should result. The concept is that if an insulating state can be obtained from a ‘ferroelectric metal’ through enhanced correlations, it would then naturally lead to magnetic ordering of the localized electron spins, coexisting polar displacements, and potentially strong ME coupling.

In this work we explore the feasibility of this approach using a combination of first-principles density functional theory (DFT) plus dynamical mean field theory (DMFT) calculations [20]. We first show that the electronic Coulomb interactions and Hund’s coupling in  $\text{LiOsO}_3$  make it an ideal candidate for realizing a Mott MF due to the multi-orbital  $t_{2g}$  physics. Next, we describe the design of a new multiferroic by control of the electronic structure through atomic scale engineering of a Mott metal-insulator transition (MIT) in an ultrashort period  $(\text{LiOsO}_3)_1/(\text{LiNbO}_3)_1$  superlattice. The insulating and magnetic state is driven by an enhancement of the electronic correlations in  $\text{LiOsO}_3$  layers owing to the kinetic energy reduction of the  $t_{2g}$  orbitals from the superlattice geometry. The ferroelectric properties mainly originate from cooperative Li and O displacements. The multiferroic phase emerges across the MIT, exhibiting a net electric polarization ( $41.2 \mu\text{C cm}^{-2}$ ) and magneti-

zation [ $0.9 \mu_B$  per formula unit (f.u.)], with calculated magnetic-ordering and ferroelectric temperatures of 671 K and 927 K, respectively. Our results uncover a promising alternative route to discovery of room-temperature multiferroics: One could search for correlated *polar metals near Mott transitions* and drive the phases into insulating states, rather than the often-pursued approach of inducing polar displacements in robustly insulating magnets.

**Calculation Details.**—We perform first-principles DFT calculations within local-density approximation (LDA) +Hubbard  $U$  method as implemented in the Vienna *Ab initio* Simulation Package (VASP) [21] with the projector augmented wave (PAW) approach and a 600 eV plane wave cutoff with a  $5 \times 7 \times 7$   $k$ -point mesh. We relax the volume and atomic positions (forces  $< 0.1$  meV  $\text{\AA}^{-1}$ ) using Gaussian smearing (20 meV width) for the Brillouin zone (BZ) integrations. We perform LDA+DMFT calculations including local Coulomb interactions parameterized by the  $U$  and the Hund's coupling  $J_h$  starting from Wannier orbitals constructed from the LDA bands [22] using an energy range spanned by the full  $d$  manifold. The impurity model is solved using Exact Diagonalization (ED) with a parallel Arnoldi algorithm [23, 24].

**Correlations in  $\text{LiOsO}_3$ .**—We first examine the effect of the interactions on the metallic state of  $\text{LiOsO}_3$  and determine the critical values for a Mott transition  $U_c$  in the paramagnetic and antiferromagnetic (AFM) phases using LDA+DMFT. The criterion for a Mott-Hubbard transition is frequently associated with the ratio between the bandwidth ( $W$ ) and the interaction strength  $U$ , so that the Mott transition occurs for  $U_c$  of the order of  $W$ . In a multiband Hubbard model with  $M$  orbitals,  $U_c$  is enhanced by orbital fluctuations, *i.e.*,  $U_c \sim \sqrt{MW}$ , [25] and it is influenced by the Hund's coupling  $J_h$ . Indeed, at half-filling,  $U_c$  is *reduced* by an enhancement of  $J_h$  [26].

In the following, we show this is precisely the situation in  $\text{LiOsO}_3$  [16]. Due to the energy separation between  $t_{2g}$  and  $e_g$  orbitals in the spectral density of state of  $\text{LiOsO}_3$  around the Fermi level, we resort to using a model for the  $t_{2g}$  levels only [16]. Owing to the symmetry breaking in bulk  $\text{LiOsO}_3$ , the orbitals in the  $d$  manifold are also permitted to mix, which lifts the degeneracy of  $t_{2g}$  orbitals with two of states remaining degenerate.

Fig. 1 shows the orbital resolved quasiparticle weight ( $Z$ ) of the occupied orbitals as a function of  $U$  for two different values of  $J_h$  for paramagnetic  $\text{LiOsO}_3$  in the experimental structure (see top panels).  $Z$  measures the metallic character of the system, and it evolves from  $Z=1$  for a non-interacting metal to  $Z=0$  for a Mott insulator. Upon increasing the value of  $J_h$ , the critical value of  $U$  required to reach the Mott state ( $Z=0$ ) is shifted to larger values of  $U$  [26].

In the correlated regime, we anticipate electron localization will lead to long-range magnetic order of the localized spins. Spin-polarized LDA+DMFT calculations, initialized with a  $G$ -type AFM structure (every spin on an Os

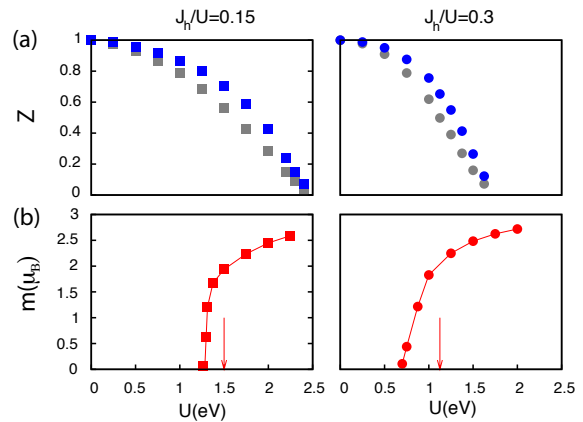


FIG. 1. (Color online) (a) Orbital resolved quasiparticle orbital weight  $Z$  (filled symbols) for paramagnetic  $\text{LiOsO}_3$  and (b) local magnetization  $m$  ( $\mu_B$ ) (obtained from a spin-polarized calculation) of the  $t_{2g}$  orbitals in  $\text{LiOsO}_3$  as function of  $U$  for different ratios of  $J_h/U$  within the LDA+DMFT calculations. Vertical arrows indicate the critical value of  $U$  required to reach the insulating state in the  $G$ -type AFM structure.

cation is antiparallel to all its neighbors), reveal that the local magnetic moment rapidly saturates to the atomic value  $S = 3/2$ . A finite magnetization also develops at intermediate  $U$  in the metallic state (Fig. 1, lower panels). The MIT, marked by vertical arrows, occurs for a weaker coupling in the AFM than in the paramagnetic state.

**Design of a Mott Multiferroic.**—The LDA+DMFT calculations reveal that a simultaneous Mott and magnetic state could be engineered in  $\text{LiOsO}_3$  by reducing the electronic kinetic energy. One avenue to control and decrease the kinetic energy relies on heterostructuring and interleaving two perovskites together to form a coherent superlattice, whereby an isostructural insulator would restrict the electron hopping due to the reduction in available channels [27–29]. Such geometries can be achieved in practice using oxide molecular-beam epitaxy or pulsed-laser deposition methods [30, 31].

Owing to the chemical and structural compatibility of  $\text{LiOsO}_3$  with  $\text{LiNbO}_3$ , with a lattice mismatch of 3.2%, we devise an ultrashort period perovskite superlattice of  $(\text{LiOsO}_3)_1/(\text{LiNbO}_3)_1$  as illustrated in panel (a) of Fig. 2. The superlattice is constructed by beginning from the  $R3c$  crystal structure of  $\text{LiOsO}_3$  ( $\text{LiNbO}_3$ ) and imposing a layered order along the  $[110]$  direction in the rhombohedral setting, which is equivalent to a  $1/1$  period  $\text{LiOsO}_3/\text{LiNbO}_3$  grown along the pseudocubic (pc)  $[001]$  direction [32]. The geometry in Fig. 2 is also different from a superlattice constructed along the  $[101]_{\text{pc}}$  direction (*c.f.*, Ref. 33), which is likely more challenging to realize experimentally. Following full relaxation of the superlattice, we find the cation order results in a symmetry reduction to the polar space group  $Pc$  with out-of-phase  $\text{OsO}_6$  and  $\text{NbO}_6$  octahedral rotations, *i.e.*, the  $a^-b^-b^-$  tilt pattern

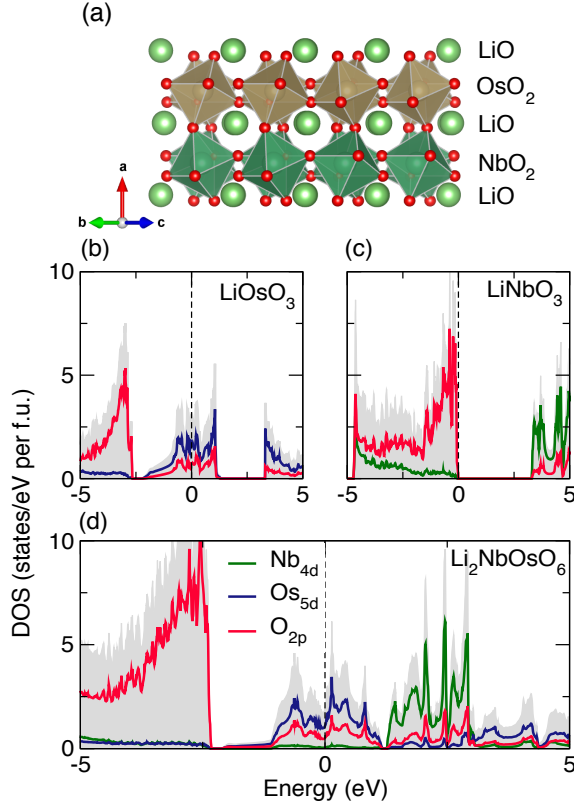


FIG. 2. (Color online) (a) The superlattice exhibits the  $a^-b^-b^-$  tilt pattern. Atom- and orbital-resolved DOS for (b)  $\text{LiOsO}_3$ , (c)  $\text{LiNbO}_3$  and (d)  $\text{LiOsO}_3/\text{LiNbO}_3$  at the DFT-LDA level.  $E_F$  is given by the (broken) vertical line at 0 eV.

given in Glazer notation [34]. The microscopic origin of polar displacements are described in detail below.

**Electronic Properties.**—Fig. 2 shows the LDA electronic density of states (DOS) for the  $\text{LiOsO}_3/\text{LiNbO}_3$  superlattice (d), compared with  $\text{LiOsO}_3$  (b) and  $\text{LiNbO}_3$  (c) using the LDA-optimized atomic structures. The results for  $\text{LiOsO}_3$  (Fig. 2b) highlight the metallic character of the former, where the weight at the Fermi level ( $E_F$ ) mainly comes from Os 5d states which show strong admixture from the O 2p states. In contrast,  $\text{LiNbO}_3$  is a band insulator, with the O 2p states forming the valence band and Nb 4d states at the conduction band minimum, separated by a gap of 3.28 eV (Fig. 2c). In the superlattice, we find essentially no charge transfer between Os and Nb: Each component ( $\text{LiOsO}_3$  and  $\text{LiNbO}_3$ ) is isoelectronic to its bulk configuration; the DOS can be described as a direct superposition of the two components (Fig. 2d). The Os 5d states partially fill the gap in the electronic spectrum formed from the the two-dimensional  $\text{NbO}_2$  planes. There is some spectral weight transfer in the vicinity of  $E_F$  among the Os orbitals, which are sensitive to the electron correlation strength as shown in Fig. 1.

We now explore the effect of electronic correlations by means of LSDA+ $U$  calculations at different values of  $U_{\text{eff}} = U - J_h$ . An accurate value of the Hubbard  $U$  is

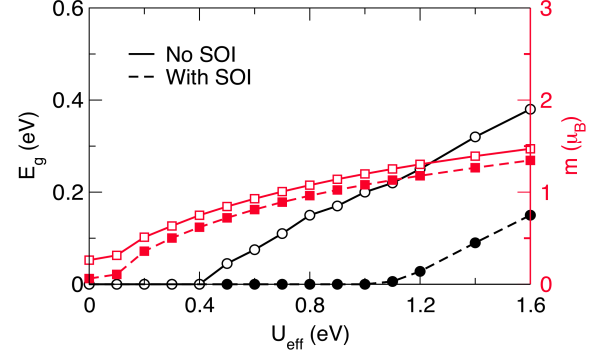


FIG. 3. (Color online) Band gap  $E_g$  and averaged local magnetic moment for Os as a function of  $U_{\text{eff}}$  with and without spin-orbit interaction (SOI).

unknown for perovskite osmates, but it is expected to be comparable to that of  $\text{NaOsO}_3$  [35] and double perovskite  $\text{Sr}_2\text{CrOsO}_6$  [36] for which a correct description of the electronic properties are obtained with  $U$  values of 1.0 and 2.0 eV, respectively. Note that the differences from various implementations of the LDA+ $U$  scheme for bulk  $\text{LiOsO}_3$  were found to be minor [16], and are anticipated to also be insignificant for the superlattice.

Fig. 3 shows the evolution in the band gap ( $E_g$ ) and magnetic moment of  $\text{Os}^{3+}$  ions ( $m$ ) as a function of the strength of  $U_{\text{eff}}$  for LSDA including spin-orbit interaction (SOI, broken lines). A gap opens at a critical  $U_{\text{eff}} \sim 1$  eV ( $U_c$ ), signaling a MIT into a magnetic insulating ground state. As expected the  $\text{LiOsO}_3/\text{LiNbO}_3$  superlattice becomes insulating for smaller values of the interaction with respect to bulk  $\text{LiOsO}_3$ . The enhancement of electronic correlations is also found for small values of  $U$ . In fact,  $\text{LiOsO}_3$  remains paramagnetic [16] while the superlattice is weakly ferrimagnetic already below  $U_c$ , where it turns into a G-type AFM insulator at  $U_{\text{eff}} \sim 0.5$  eV.

The reduction in  $U_c$  for the MIT in the superlattice can be understood by analyzing the effect of the geometrical confinement on the  $t_{2g}$  band dispersions. (For simplicity, we use the LDA electronic structures given in Ref. 32.) While the bandwidth of the  $d_{xy}$  orbitals is essentially the same as for bulk  $\text{LiOsO}_3$ , the  $d_{xz}$  and  $d_{yz}$  bands in  $\text{LiOsO}_3/\text{LiNbO}_3$  are significantly narrowed as a consequence of the reduced hopping along the superlattice direction. This leads to a reduction of the kinetic energy which enhances the electron-electron correlations, making the superlattice a Mott insulator at moderate interaction strengths. We note that when SOI are excluded in the calculations (Fig. 3, solid lines), the MIT occurs at a further reduced correlation strength ( $U_c \sim 0.5$  eV), and the magnetic moment only slightly increases. Such behaviors are also observed in bulk  $\text{LiOsO}_3$  [16].

**Ferroelectric Polarization.**—We now apply a group the-

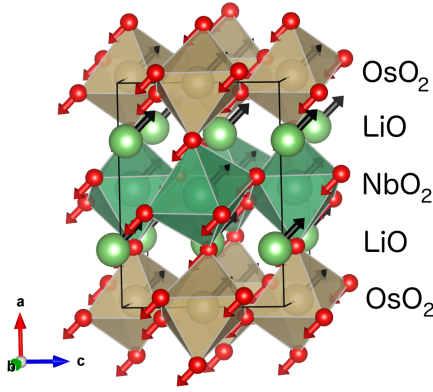


FIG. 4. (Color online) Illustration of the polar zone-center mode along the  $[101]$ -direction labeled by irrep  $\Gamma_2^-$ . Anti-polar displacements along the  $[010]$ -direction are omitted for clarity.

oretical analysis [37, 38] of the  $\text{LiOsO}_3/\text{LiNbO}_3$  structure to understand the inversion symmetry-breaking displacements that produce the  $Pc$  ground state. We use a fictitious  $P2_1/c$  centrosymmetric phase (where polar displacements are switched off) as the reference phase from which the symmetry-adapted mode displacements are obtained as different irreducible representations (irreps) of the  $P2_1/c$  space group operators [39]. We find the loss of inversion symmetry mainly derives from cooperative Li and O displacements in the  $(101)$  mirror plane of the  $Pc$  phase. Moreover, we find anti-polar displacements along the  $b$ -axis which result in no net polarization. All polar displacements are described by a distortion vector that corresponds to the irrep  $\Gamma_2^-$  along the  $[101]$ -direction of the  $Pc$  structure (Fig. 4). These displacements are consistent with the acentric Li and O ionic displacements identified to be responsible for lifting inversion symmetry in bulk  $\text{LiOsO}_3$  [10, 13] and across the ferroelectric transition in  $\text{LiNbO}_3$  [40].

We now compute the ferroelectric polarization in  $\text{LiOsO}_3/\text{LiNbO}_3$  using the Berry’s phase approach [41] within LSDA+ $U$  ( $U_c = 0.5 \text{ eV}$ ). The spontaneous electric polarization of the  $Pc$  phase is  $32.3 \mu\text{C cm}^{-2}$  and  $25.5 \mu\text{C cm}^{-2}$  along the  $[100]$ -direction, *i.e.*, along the pseudo-cubic  $[001]$  superlattice repeat direction and  $[001]$ -directions, respectively. (Note that the  $[101]$ -direction in  $\text{LiOsO}_3/\text{LiNbO}_3$  corresponds to the polar  $[111]$ -direction in  $\text{LiNbO}_3$ .) Together this yields a net polarization along the  $[101]$ -direction of  $41.2 \mu\text{C cm}^{-2}$ . These values are also robust to SOI, with a change of less than 15% to value of the total polarization. Following the recipe of Ref. 42, we use the energy difference between the high-symmetry ( $P2_1/c$ ) and low-symmetry ( $Pc$ ) to obtain a ferroelectric Curie temperature of 927 K for the superlattice. This value is close to the extrapolated transition temperature for  $\text{LiNbO}_3$  ( $>1,400 \text{ K}$ ) [43], and far exceeds that of bulk  $\text{LiOsO}_3$  where inversion symmetry is lost near 140 K [10].

*Magnetic Ordering Temperature.*—Our DMFT calcula-

tions indicate that when the superlattice material enters in the Mott state the magnetic moment is  $\sim 3\mu_B$ , corresponding to a high-spin  $S = 3/2$  state. We now estimate the Néel temperature for  $\text{LiOsO}_3/\text{LiNbO}_3$  by extracting the exchange interaction constants from spin-polarized DFT energies computed at  $U_c$  without SOI following the approach in Ref. 44. Assuming that the magnetism arises by ordering such localized spins, we obtain intra- and inter-plane Os–Os exchange magnetic couplings of  $-5.6 \text{ meV}$  and  $-0.2 \text{ meV}$  respectively, where a negative interaction indicate AFM exchange. From these values and without Anderson’s renormalization [45], we estimate a Néel temperature of 671 K for the  $\text{LiOsO}_3/\text{LiNbO}_3$  superlattice, which makes the material a correlation-induced room-temperature multiferroic.

*Conclusions.*—We used a LDA+DMFT approach to study the electronic properties of the “ferroelectric” metal  $\text{LiOsO}_3$ . A detailed understanding of the electronic structure of  $\text{LiOsO}_3$  shows that a reduction of the kinetic energy can drive the system into a Mott insulating state. We use this concept to propose a strategy to design multiferroic materials by constructing a superlattice with the uncorrelated polar  $\text{LiNbO}_3$  dielectric. On the basis of LSDA+ $U$  calculations we show that the ultra-short period  $\text{LiOsO}_3/\text{LiNbO}_3$  superlattice should be a type-I room-temperature Mott multiferroic with a large  $41.2 \mu\text{C cm}^{-2}$  electric polarization.

The large ferroelectric displacements from the  $\text{LiNbO}_3$  layers facilitate the high ferroelectric ordering temperature in the  $\text{LiOsO}_3/\text{LiNbO}_3$  heterostructure as observed from the similarity in the Curie temperature of the superlattice with that of  $\text{LiNbO}_3$ . In this case  $\text{LiOsO}_3/\text{LiNbO}_3$  would behave as a paramagnetic Mott ferroelectric at high temperatures and transition into Mott multiferroic below the Néel temperature, which is predicted to be well-above room temperature. Because the exchange interactions of Os are mediated by the coordinating O ligands, which are essential to and produce the ferroelectric distortion, a strong ME coupling is anticipated as in  $\text{Sr}_{1-x}\text{Ba}_x\text{MnO}_3$  [7–9]. We hope this work motivates the synthesis of new artificial multiferroics, and adds to the growing discussion of new applications where noncentrosymmetric metals and ferroelectric materials may be united.

GG and MC acknowledge financial support by the European Research Council under FP7/ERC Starting Independent Research Grant “SUPERBAD” (Grant Agreement No. 240524). DP and JMR acknowledge the ARO under Grant Nos. W911NF-12-1-0133 and W911NF-15-1-0017 for financial support and the HPCMP of the DOD for computational resources.

- 
- [1] T. Kimura et al. , Nature (London) **426**, 55 (2003).
  - [2] N. Hur et al. , Nature (London) **429**, 392 (2004).



- [3] J. Wang et al. , Science **299**, 1719 (2003).
- [4] R. G. Pearson, Journal of Molecular Structure: THEOCHEM **103**, 25 (1983).
- [5] S.-W. Cheong and M. Mostovoy, Nat. Mat. **6**, 13 (2007).
- [6] Sanghyun Lee, M. T. Fernandez-Diaz, H. Kimura, Y. Noda, D. T. Adroja, Seongsu Lee, Junghwan Park, V. Kiryukhin, S.-W. Cheong, M. Mostovoy, and Je-Geun Park Phys. Rev. B **88**, 060103(R) (2013)
- [7] H. Sakai, J. Fujioka, T. Fukuda, D. Okuyama, D. Hashizume, F. Kagawa, H. Nakao, Y. Murakami, T. Arima, A. Q. R. Baron, Y. Taguchi, and Y. Tokura, Phys. Rev. Lett. **107**, 137601 (2011)
- [8] G. Giovannetti, S. Kumar, C. Ortix, M. Capone, and J. van den Brink, Phys. Rev. Lett. **109**, 107601 (2012).
- [9] R. Nourafkan, G. Kotliar, and A.-M. S. Tremblay, Phys. Rev. B **90**, 220405(R) (2014)
- [10] Y. Shi, Y. Guo, X. Wang, A. J. Princep, D. Khalyavin, P. Manuel, Y. Michiue, A. Sato, K. Tsuda, S. Yu, M. Arai, Y. Shirako, M. Akaogi, N. Wang, K. Yamaura and A. T. Boothroyd , Nat. Mat. **12**, 1024 (2013).
- [11] P. W. Anderson and E. I. Blount, Phys. Rev. Lett. **14**, 217 (1965).
- [12] Q. Yao, H. Wu, K. Deng, and E. Kan, RSC Adv. **4**, 26843 (2014)
- [13] Sim Hyunsu and Kim Bog G., Phys. Rev. B **89** 201107 (2014).
- [14] H. Boysen and F. Altorfer, Acta Crystallogr. B **50**, 405 (1994).
- [15] H.D. Megaw, Acta Crystallogr. Section A **24**, 583 (1968).
- [16] G. Giovannetti and M. Capone, Phys. Rev. B **90**, 195113 (2014)
- [17] H. Sim and B. G. Kim, Phys. Rev. B **89**, 201107(R) (2014).
- [18] I. Inbar and R. E. Cohen, Phys. Rev. B **53**, 1193 (1996).
- [19] D. Puggioni and J. M. Rondinelli, Nat. Commun. **5**, 3432 (2014).
- [20] A. Georges, G. Kotliar, W. Krauth, and M. J. Rozenberg, Rev. Mod. Phys. **68**, 13 (1996).
- [21] G. Kresse and J. Furthmuller, Phys. Rev. B **54**, 11 169 (1996); Comput. Mater. Sci. **6**, 15 (1996).
- [22] A. A. Mostofi, J. R. Yates, Y.-S. Lee, I. Souza, D. Vanderbilt and N. Marzari, Comput. Phys. Commun. **178**, 685 (2008).
- [23] M. Capone, L. de' Medici, and A. Georges, Phys. Rev. B **76**, 245116 (2007).
- [24] R. B. Lehoucq, D. C. Sorensen, and C. Yang, ARPACK Users' Guide (SIAM, Philadelphia, 1997).
- [25] O. Gunnarsson, E. Koch, and R. Martin, Phys. Rev B **54** R11026 (1996)
- [26] A. Georges, L. de' Medici, J. Mravlje, Annual Reviews of Condensed Matter Physics **4**, 137-178 (2013).
- [27] B. Gray, H.N. Lee Ho, J. Liu, J. Chakhalian, and J.W. Freeland, Appl. Phys. Lett. **97** 013105 (2010).
- [28] S. Middey, D. Meyers, M. Kareev, E. J. Moon, B. A. Gray, X. Liu, J. W. Freeland, and J. Chakhalian, Appl. Phys. Lett. **101** 261602 (2012).
- [29] S. Middey, P. Rivero, D. Meyers, M. Kareev, X. Liu, Y. Cao, J.W. Freeland, S. Barraza-Lopez, and J. Chakhalian, Sci. Rep **4** 6819 (2014).
- [30] D. G. Schlom, L.-Q. Chen, X. Pan, A. Schmehl, and M.A. Zurbuchen, J. Amer. Ceram. Soc. **91** 2429 (2008).
- [31] Blok J. L., Wan X., Koster, G., Blank D. H. A. and Rijnders G., Appl. Phys. Lett. **99** 151917 (2011).
- [32] See Supplemental Material at [URL will be inserted by publisher] for discussion of the superlattice construction, equilibrium atomic positions using the LDA and LSDA+ $U$  with  $U = 0.5$  eV, and additional electronic structures. Note for simplicity, we assume  $\alpha = \beta = \gamma = 90^\circ$  which slightly shifts the results by few percent, but the constraint is anticipated to be appropriate for coherent epitaxial growth.
- [33] H. J. Xiang, Phys. Rev. B **90**, 094108 (2014).
- [34] A. M. Glazer, Acta Cryst. A **31**, 756 (1975)
- [35] Y. G. Shi, Y. F. Guo, S. Yu, M. Arai, A. A. Belik, A. Sato, K. Yamaura, E. Takayama-Muromachi, H. F. Tian, H. X. Yang, J. Q. Li, T. Varga, J. F. Mitchell, and S. Okamoto, Phys. Rev. B **80**, 161104(R) (2009).
- [36] O. Nganba Meetei, Onur Erten, Mohit Randeria, Nandini Trivedi, and Patrick Woodward, Phys. Rev. Lett. **110**, 087203 (2013).
- [37] D. Orobengoa, C. Capillas, M. I. Aroyo, and J. M. Perez-Mato, Journal of Applied Crystallography **42**, 820 (2009).
- [38] J. M. Perez-Mato, D. Orobengoa, and M. I. Aroyo, Acta Cryst. A **66**, 558 (2010).
- [39] The ferroelectric transition in  $\text{LiOsO}_3$  and  $\text{LiNbO}_3$  is  $R\bar{3}c \rightarrow R3c$ . Using the same method described in the main paper for the construction of the superlattice but starting from the  $R\bar{3}c$  crystal structure of  $\text{LiOsO}_3$  ( $\text{LiNbO}_3$ ) the atomic relaxation of the 'idealized' superlattice gives the centrosymmetric  $P21/c$  phase. This structure is used as the reference for both the mode decomposition and in the calculation of the ferroelectric Curie temperature.
- [40] N. A. Benedek, and C. J. Fennie, The Journal of Physical Chemistry C **117** 13339 (2013)
- [41] R.D. King-Smith and D. Vanderbilt, Phys. Rev. B **47**, 1651 (1993); D. Vanderbilt and R. D. Smith, Phys. Rev. B **48**, 4442 (1993).
- [42] Jacek C. Wojdel and Jorge Íñiguez, arXiv:1312.0960.
- [43] G. A. Smolenskii, N. N. Krainik, N. P. Khuchua, V. V. Zhdanova, and I. E. Mylnikova, phys. stat. sol. (b) **13**, 309 (1966).
- [44] N. Lampis, C. Franchini, G. Satta, A. Geddo-Lehmann, and S. Massidda, Phys. Rev. B **69**, 064412 (2004).
- [45] P. W. Anderson, Phys. Rev. **115**, 2 (1959)

# Design of a Mott Multiferroic from a Non-Magnetic Polar Metal

## Supplementary Materials

---

- [1] H. T. Stokes and D. M. Hatch, "FINDSYM: Program for Identifying the Space Group Symmetry of a Crystal." J. Appl. Cryst. **38**, 237-238 (2005), ISOTROPY Software Suite, <http://iso.byu.edu>.

TABLE I. Calculated crystallographic parameters for  $R3c$   $\text{LiOsO}_3$  using LDA functional.

<b><math>\text{LiOsO}_3</math></b>		$a = b = 4.9399 \text{ \AA}, c = 13.3019 \text{ \AA}$		
$R3c$		$\alpha = \beta = 90^\circ, \gamma = 120^\circ$		
Atom	Wyck. Site	$x$	$y$	$z$
Li	$6a$	0	0	0.61117
Os	$6b$	0	0	0.32084
O	$18b$	-0.00388	0.36259	0.06825

TABLE II. Calculated crystallographic parameters for  $R3c$   $\text{LiNbO}_3$  using LDA functional.

<b><math>\text{LiNbO}_3</math></b>		$a = b = 5.1052 \text{ \AA}, c = 13.7472 \text{ \AA}$		
$R3c$		$\alpha = \beta = 90^\circ, \gamma = 120^\circ$		
Atom	Wyck. Site	$x$	$y$	$z$
Li	$6a$	0	0	0.61517
Nb	$6b$	0	0	0.33169
O	$18b$	-0.01367	0.35987	0.06330

TABLE III. Calculated crystallographic parameters for  $Pc$   $\text{Li}_2\text{NbOsO}_6$  using the LDA functional.

<b><math>\text{LiOsO}_3/\text{LiNbO}_3</math></b>		$a = 7.35270 \text{ \AA}, b = 5.02739 \text{ \AA}, c = 5.36541 \text{ \AA}$		
$Pc$		$\alpha = \gamma = 90^\circ, \beta = 95.109^\circ$		
Atom	Wyck. Site	$x$	$y$	$z$
Li1	$2a$	0.27896	0.25751	0.45909
Li2	$2a$	0.78342	0.74972	-0.07013
Nb	$2a$	-0.00633	0.25287	0.00169
Os	$2a$	0.49713	0.75123	0.53150
O1	$2a$	0.23965	0.12376	0.02510
O2	$2a$	0.73578	0.60514	0.54599
O3	$2a$	-0.09599	0.05685	0.71217
O4	$2a$	0.41768	0.54538	0.23192
O5	$2a$	0.04578	0.58866	0.85929
O6	$2a$	0.54412	0.04168	0.32305

TABLE IV. Calculated crystallographic parameters for  $Pc$   $\text{Li}_2\text{NbOsO}_6$  without monoclinic angle using the LDA functional.

<b><math>\text{LiOsO}_3/\text{LiNbO}_3</math></b>		$a = 7.35884 \text{ \AA}, b = 5.03159 \text{ \AA}, c = 5.36989 \text{ \AA}$		
$Pc$		$\alpha = \beta = \gamma = 90^\circ$		
Atom	Wyck. Site	$x$	$y$	$z$
Li1	$2a$	0.27310	0.26765	0.47516
Li2	$2a$	0.78081	0.75357	-0.05429
Nb	$2a$	-0.00421	0.25110	0.00188
Os	$2a$	0.49815	0.75234	0.52637
O1	$2a$	0.24071	0.12246	0.01238
O2	$2a$	0.73609	0.60651	0.54411
O3	$2a$	-0.09326	0.05556	0.71992
O4	$2a$	0.41773	0.53696	0.24015
O5	$2a$	0.04603	0.58671	0.85024
O6	$2a$	0.54504	0.03169	0.30376

TABLE V. Calculated crystallographic parameters for  $Pc$   $\text{Li}_2\text{NbOsO}_6$  without monoclinic angle using the LSDA+ $U$  with  $U=U_c=0.5$  eV.

$\text{LiOsO}_3/\text{LiNbO}_3$				$a = 7.35714 \text{ \AA}, b = 5.03042 \text{ \AA}, c = 5.36865 \text{ \AA}$
$Pc$				$\alpha = \beta = \gamma = 90^\circ$
Atom	Wyck. Site	$x$	$y$	$z$
Li1	$2a$	0.27431	0.26460	0.47149
Li2	$2a$	0.77680	0.75646	-0.05271
Nb	$2a$	-0.00460	0.25150	0.00212
Os	$2a$	0.49708	0.75063	0.52604
O1	$2a$	0.24114	0.12241	0.01487
O2	$2a$	0.73596	0.60719	0.54175
O3	$2a$	-0.09280	0.05536	0.72002
O4	$2a$	0.41875	0.54274	0.23604
O5	$2a$	0.04702	0.58598	0.84961
O6	$2a$	0.54653	0.03942	0.31046

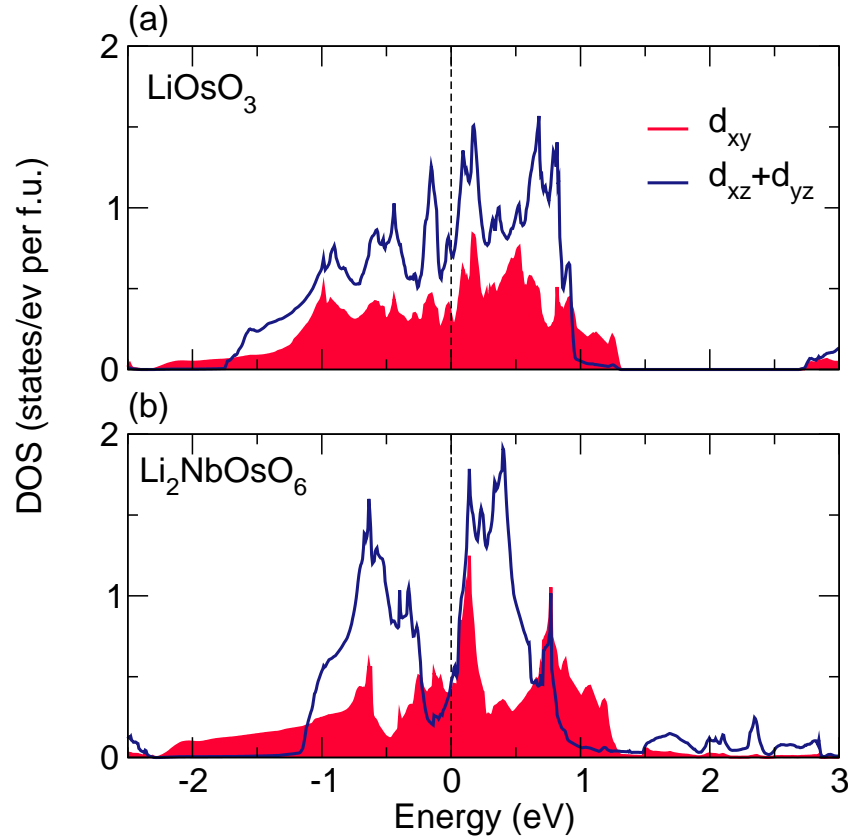


FIG. 5. (Color online) Resolved  $5d$   $t_{2g}$  states of Os for (a)  $\text{LiOsO}_3$  and (b)  $\text{Li}_2\text{NbOsO}_6$  within LDA. The bandwidth of the  $d_{xy}$  orbitals for bulk  $\text{LiOsO}_3$  and  $\text{Li}_2\text{NbOsO}_6$  are the same while in the superlattice the  $d_{xz}$  and  $d_{yz}$  orbitals have a reduced bandwidth.



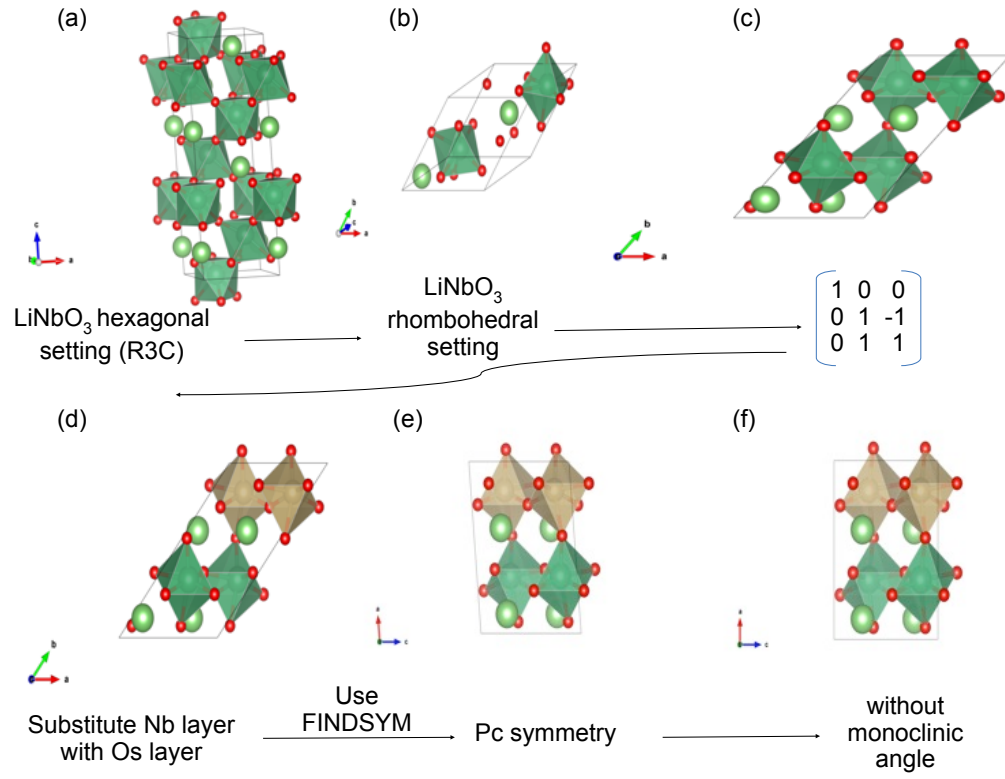


FIG. 6. (Color online) Superlattice construction: (a) Starting from the *R3c* crystal structure of LiNbO<sub>3</sub> in the hexagonal setting with 30 atoms, (b) we transform to the rhombohedral setting with 10 atoms. (c) Next we double the cell with the transformation matrix and (d) substitute a NbO<sub>2</sub> layer with OsO<sub>2</sub> layer. (e) We identify the new space group *Pc* with FINDSYM [1] and finally (f) we set the monoclinic angle to 90°.